

# Supramolecular Peptide Nanofibrils with Optimized Sequences and Molecular Structures for Efficient Retroviral Transduction

Stefanie Sieste, Thomas Mack, Edina Lump, Manuel Hayn, Desiree Schütz, Annika Röcker, Christoph Meier, Kübra Kaygisiz, Frank Kirchhoff, Tuomas P. J. Knowles, Francesco S. Ruggeri,\* Christopher V. Synatschke,\* Jan Münch,\* and Tanja Weil\*

Amyloid-like peptide nanofibrils (PNFs) are abundant in nature providing rich bioactivities and playing both functional and pathological roles. The structural features responsible for their unique bioactivities are, however, still elusive. Supramolecular nanostructures are notoriously challenging to optimize, as sequence changes affect self-assembly, fibril morphologies, and biorecognition. Herein, the first sequence optimization of PNFs, derived from the peptide enhancing factor-C (EF-C, QCKIKQIINMWQ), for enhanced retroviral gene transduction via a multiparameter and a multiscale approach is reported. Retroviral gene transfer is the method of choice for the stable delivery of genetic information into cells offering great perspectives for the treatment of genetic disorders. Single fibril imaging, zeta potential, vibrational spectroscopy, and quantitative retroviral transduction assays provide the structure parameters responsible for PNF assembly, fibrils morphology, secondary and quaternary structure, and PNF-virus-cell interactions. Optimized peptide sequences such as the 7-mer, CKFKFQF, have been obtained quantitatively forming supramolecular nanofibrils with high intermolecular  $\beta$ -sheet content that efficiently bind virions and attach to cellular membranes revealing efficient retroviral gene transfer.

## 1. Introduction

Peptide nanofibrils (PNFs) are ubiquitous in nature. They are formed by spontaneous self-assembly and exert many vital functions in living organisms. Peptide nanofibrils consisting of regular cross- $\beta$  sheet structures, often termed amyloid-like structures,<sup>[1–4]</sup> feature many outstanding properties such as high rigidity, tensile strength, and enhanced resistance towards biodegradation.<sup>[5,6]</sup> They play both functional and pathological roles in many living organisms: Serving as templates for melanin biosynthesis,<sup>[7]</sup> for hormone storage,<sup>[8]</sup> participating in spermatozoa selection and clearance,<sup>[9]</sup> or constituting the fibrillar curli structures of *Escherichia coli* promoting their surface adhesion.<sup>[10]</sup> Their formation has also been associated with numerous human diseases (around 50), such as Alzheimer's disease or Diabetes

S. Sieste, T. Mack, K. Kaygisiz, Dr. C. V. Synatschke, Prof. T. Weil  
 Department Synthesis of Macromolecules  
 Max Planck Institute for Polymer Research  
 Ackermannweg 10, 55128 Mainz, Germany  
 E-mail: synatschke@mpip-mainz.mpg.de; weil@mpip-mainz.mpg.de  
 S. Sieste, T. Mack, Prof. T. Weil  
 Institute of Inorganic Chemistry I  
 Ulm University  
 Albert-Einstein-Allee 11, 89081 Ulm, Germany  
 Dr. E. Lump, M. Hayn, D. Schütz, Dr. A. Röcker,  
 Prof. F. Kirchhoff, Prof. J. Münch  
 Institute of Molecular Virology  
 Ulm University Medical Center  
 Meyerhofstraße 1, Ulm 89081, Germany  
 E-mail: jan.muensch@uni-ulm.de

 The ORCID identification number(s) for the author(s) of this article can be found under <https://doi.org/10.1002/adfm.202009382>.

© 2021 The Authors. Advanced Functional Materials published by Wiley-VCH GmbH. This is an open access article under the terms of the Creative Commons Attribution License, which permits use, distribution and reproduction in any medium, provided the original work is properly cited.

DOI: [10.1002/adfm.202009382](https://doi.org/10.1002/adfm.202009382)

Dr. C. Meier  
 Institute of Organic Chemistry III/Macromolecular Chemistry  
 Ulm University  
 Albert-Einstein-Allee 11, 89081 Ulm, Germany  
 Prof. T. P. J. Knowles, Prof. F. S. Ruggeri  
 Department of Chemistry  
 University of Cambridge  
 Cambridge CB2 1EW, UK  
 E-mail: simone.ruggeri@wur.nl  
 Prof. T. P. J. Knowles  
 Cavendish Laboratory  
 University of Cambridge  
 Cambridge CB3 0HE, UK  
 Prof. F. S. Ruggeri  
 Laboratory of Organic and Physical Chemistry  
 Wageningen University  
 Stippeneng 4, Wageningen 6703 WE, The Netherlands  
 Prof. J. Münch  
 Core Facility of Functional Peptidomics  
 Ulm University Medical Center  
 Albert-Einstein-Allee 47, 89081 Ulm, Germany

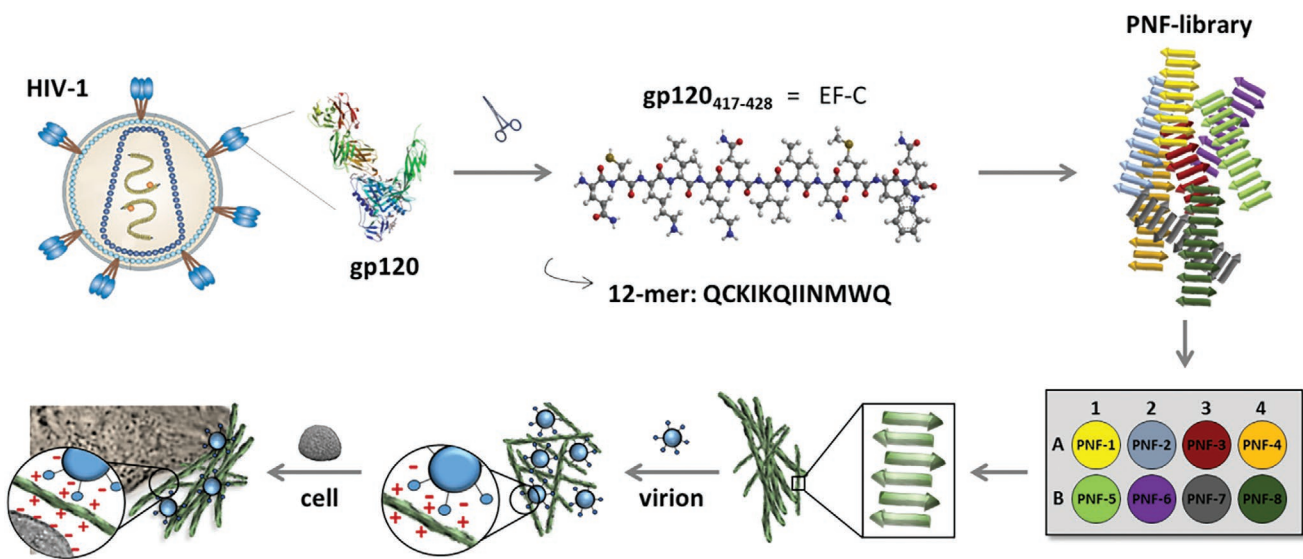


**Figure 1.** Schematic illustration of the structure–activity study of transduction enhancing PNFs. EF-C is a bioactive fragment of the HIV-1 glycoprotein gp120 that forms PNFs and enhances viral transduction. Through multiparameter and multiscale optimization, a library of EF-C derived peptides was synthesized. The library was evaluated for fibril formation, structural parameters, virion-PNF-cell interactions, and viral transduction enhancement.

mellitus type 2.<sup>[11]</sup> We have previously shown that PNF formation is also common in semen from healthy human individuals because semen contains an abundance of amyloidogenic fragments of prostate acidic phosphatase and the semenogelins 1 and 2.<sup>[12,13]</sup> PNFs likely play important roles in innate immunity and in eliminating poor-quality sperm upon deposition in the female reproductive tract.<sup>[9]</sup> In addition, semen PNFs enhance the infectivity of human immunodeficiency virus-1 (HIV-1), herpesviruses 1 and 2 and Ebola virus, and may increase the transmission potential of these sexually transmitted pathogens.<sup>[14,15]</sup>

The rich bioactivity of endogenous amyloids has inspired scientists to elucidate structural features crucial for their broad functions. Moreover, understanding their specific interactions of PNF with cellular membranes and viruses is not only of great fundamental interest but also essential to design new nanomaterials for medicine, for example, to enhance retroviral gene transfer.<sup>[16–18]</sup> Retroviral gene transfer is the method of choice for the delivery of genetic material into cells offering great perspectives for the treatment of genetic disorders, malignancies, and infectious diseases.<sup>[19,20]</sup> Until now,  $\gamma$ -retroviral and lentiviral vectors (herein both referred to as retroviral vectors) have been used in more than 478 gene therapy clinical trials<sup>[21]</sup> allowing stable, long-lasting gene expression. HIV-1 based lentiviral vectors even allow transduction of non-dividing cells,<sup>[22,23]</sup> which is essential to treat, that is, metachromatic leucodystrophy or inherited primary immunodeficiencies with a significant clinical benefit.<sup>[24,25]</sup> However, major challenges in retroviral gene delivery need to be overcome such as low transduction efficiencies due to: i) low concentrations of transducing particles in the viral vector stock; and ii) low efficiency of virion attachment to the target cell. Nowadays, retroviral gene delivery is often promoted by a combination of spin-infection and utilization of RetroNectin, a long polypeptide, consisting of 574 amino acid and a fibronectin derivative that colocalizes with virions and cells.<sup>[26–29]</sup> The large scale use of RetroNectin

is limited by its high costs and even more importantly, it has to be coated onto plates or the inner surface of culture bags to capture virions, requiring several washing steps<sup>[30–32]</sup> which impedes *in vivo* applications.<sup>[33]</sup>

PNFs have been reported as powerful alternatives to RetroNectin as they enhance retroviral gene transfer with a similar efficiency but do not require coating.<sup>[18,34,35]</sup> We discovered the self-assembling 12-mer peptide EF-C (QCKIKQIINMWQ) corresponding to residues 417–428 of the HIV envelope protein gp120 (Figure 1).<sup>[18]</sup> EF-C PNFs efficiently concentrate virus stock solutions and increase cell attachment as well as retroviral gene transfer into hematopoietic stem cells and T cells by different types of vectors *in vitro* and *ex vivo*, which holds various opportunities for gene therapy approaches, in particular chimeric antigen receptor T cell (CAR-T) immunotherapy.<sup>[18,34–36]</sup> Compared to other PNFs and known transduction enhancers, EF-C reveals one of the highest enhancing effects on retroviral gene transfer and has been commercialized under the brand name Protransduzin.<sup>[34]</sup>

Very little is known about the structural features of bioactive PNFs such as EF-C, which severely limits rational approaches to further optimize their bioactivity. To the best of our knowledge, no structure–activity study of supramolecular nanofibrils has been reported yet. This limitation is due to the fact that supramolecular nanostructures are notoriously challenging to optimize as multiple parameters affect self-assembly, fibril morphologies, and biorecognition and the involved structures cover several length scales from the molecular to the mesoscopic regime. A limited number of studies have investigated small sequence variations in amyloid PNFs on transduction enhancement.<sup>[37–40]</sup> However, rational approaches that unravel structure–morphology–bioactivity relationships of PNF are still elusive. Herein, we report the first sequence optimization of PNFs for enhanced retroviral gene transduction via a rational multiparameter-based approach. The amino acids and peptide motifs within PNFs responsible for self-assembly, fibrils

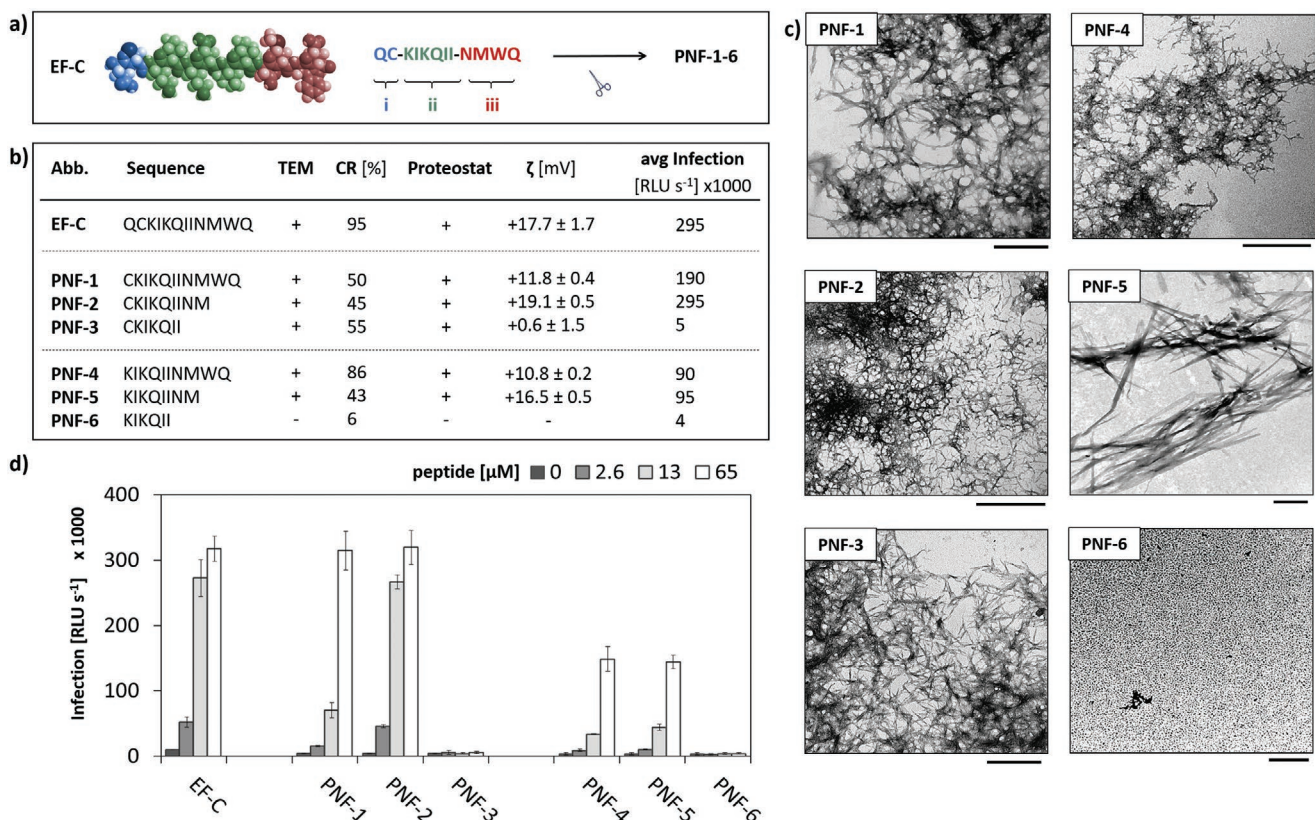


**Figure 2.** PNF library generation upon sequence truncation of EF-C. a) EF-C was subdivided into three domains: i) QC; ii) KIKQII; and iii) NMWQ. b) Impact of sequence variations on peptide self-assembly (with + = fibrils and - = no aggregate formation detected), monomer-to-fibril conversion rates (CR) and transduction enhancement. Proteostat emission indicates accessible cross  $\beta$ -sheet binding pockets in the fibril core and indicated PNFs with + = Proteostat activity and - = no Proteostat fluorescence observed.  $\zeta$ -potential values for PNF solutions. Average (avg) RLU s<sup>-1</sup> in infectivity assay for 13–65  $\mu$ M. c) Representative TEM micrographs of PNF-1 to PNF-5 reveal the formation of fibrillar aggregates. No aggregates were observed for PNF-6. The scale bars represent 500 nm. d) HIV-1 infection rates of TZM-bl cells observed in the presence of increasing concentrations of PNF. Shown are mean values derived from triplicate infections  $\pm$  standard deviation. RLU s<sup>-1</sup>; relative light units per second.

morphology, secondary and quaternary structure, and virus and/or cell binding were identified. We believe that unravelling the structural parameters of PNFs responsible for their unique bioactivities paves the way to a fundamental understanding of the rich bioactivity of PNFs and ultimately addresses the great need for improved nanomaterials for clinical applications, for example, in gene therapy.

EF-C served as a starting point for multiparameter optimization. Its sequence was first divided into smaller fragments to identify amino acids and amino acid patterns responsible for assembly and interaction with virions or cellular membranes. Subsequently, several focused peptide libraries were synthesized as depicted in Figure 2a. EF-C features: i) a short N-terminal QC fragment; ii) an amphiphilic KIKQII domain; and iii) a C-terminal NMWQ sequence. The C-terminal NMWQ domain represents a fragment of the  $\beta$ 20/21 strand in the gp120 HIV-1 envelope protein region that has been proposed to constitute the primary HIV binding site for the CD4 receptors of immune cells<sup>[41]</sup> and to play a crucial role for the transduction enhancement of PNFs. The hexameric KIKQII fragment features an amphiphilic pattern with three hydrophobic isoleucine (I) and two positively charged lysine (K) residues. The lipophilic (I) residues could promote self-assembly, whereas the

hydrophilic and positively charged (K) residues provide solubility for stabilizing the superstructures in aqueous media.<sup>[15,17]</sup>

PNF formation was achieved by dilution from a dimethyl sulfoxide stock solution to PBS buffer and aggregation was confirmed by transmission electron microscopy (TEM). Conversion rates (CR) from the soluble peptide monomers to supramolecular PNFs were quantified as published previously.<sup>[42]</sup>  $\zeta$ -potential measurements were performed to determine the charge of PNF assemblies; secondary and quaternary structures of PNFs were characterized by infrared spectroscopy and intermolecular  $\beta$ -sheet structures and were confirmed by the blue-shifted emission of Proteostat<sup>[43]</sup> (Figure S1, Table S1, Supporting Information). The transduction enhancing properties of the PNFs were evaluated in infection experiments using HIV-1 particles as prototype retroviral vectors. Virions were exposed to increasing concentrations of PNFs and the mixtures were used to infect TZM-bl reporter cells,<sup>[44]</sup> which are widely used to study HIV infection rates. These cells are genetically engineered to express the HIV receptors CD4 and CXCR4/CCR5 and contain a stably integrated  $\beta$ -galactosidase gene under the control of the viral long terminal repeat promoter region. Upon successful infection, the HIV-1 transactivator Tat protein is expressed and turns on the viral promoter resulting in  $\beta$ -galactosidase production, which

was quantified in a chemiluminescence-based assay performed 72 h post infection. None of the peptides tested in this study affected cell viability within the concentrations used for transduction studies (Figure S2, Supporting Information).

## 2. Results

### 2.1. PNF Library Generation upon Sequence Truncation

EF-C instantaneously forms positively charged PNFs ( $\zeta = +17.7$  mV) with high conversion rates (CR: 95%) and it is used as an internal standard to compare the infectivity enhancement of the peptide nanofibrils in different sets of experiments, that is, on different days. Several studies have shown that even short peptide sequences can exhibit robust fibril formation.<sup>[45,46]</sup> We therefore envisioned the identification of EF-C derived peptides with fewer than 13 amino acids that retain high transduction enhancement. After deleting the N-terminal glutamine (Q) and stepwise truncation of the C-terminal residues, PNF-1 (CKIKQIINMWQ), PNF-2 (CKIKQIINM), and PNF-3 (CKIKQII) still formed fibrils but with moderate CRs (45–55%) independent of the length of the C-terminal NMWQ fragment (Figure 2b,c). The transduction efficiencies of PNF-1 and PNF-2 with positive  $\zeta$ -potentials were comparable to EF-C (at 65  $\mu$ M, corresponding to 200  $\mu$ g mL<sup>-1</sup> EF-C, Figure 2d), whereas the almost neutral ( $\zeta = +0.6$  mV) PNF-3 without the NMWQ fragment was inactive.

After deletion of the (QC) sequence, PNF-4 (KIKQIINMWQ) still assembled with high CR (86%) and PNF-5 (KIKQIINM) with moderate CR (43%, Figure 2b,c). A time-dependent measurement of the  $\zeta$ -potential of PNF-4 and PNF-16 over 30 days revealed no significant changes in the respective  $\zeta$ -potential values (Figure S3, Supporting Information). Interestingly, positively charged PNF-4 and PNF-5, which lack the cysteine residue, were considerably less active than PNF-1 and PNF-2 despite their positive  $\zeta$ -potentials and comparable CRs. PNF-6 (KIKQII) did not form fibrils and showed no activity. These data gave a first indication that significant transduction enhancement requires: i) PNF formation; ii) positive  $\zeta$ -potentials; and iii) an N-terminal cysteine residue.

### 2.2. Optimized Amphiphilic Pattern Improves Fibril Formation

In polar solvents, the morphology of intermolecular  $\beta$ -sheet rich aggregates is driven by the formation of a bilayer structure, where hydrophobic domains form the fibril core and the hydrophilic side chains arrange at the surface of the fibrillar backbone.<sup>[18]</sup> In order to improve the packing of the peptides in the PNFs, we altered: i) the arrangement of the hydrophilic and lipophilic amino-acids within the peptide sequences; ii) replaced the lipophilic (I) residues by other hydrophobic amino acids; and iii) identified minimal sequences with high CRs and transduction enhancement.<sup>[47,48]</sup> The central amphiphilic PNF-6 (KIKQII) fragment of the EF-C sequence reveals two structural defects in its sequence as the second (I) residue of KIKQII faces an opposite direction to the other two (I)-residues and the polar (Q) is located adjacent to the unpolar (I) and also opposite

to the polar (K) residues (Figure 3a, blue model). By switching the positions of (Q) and its neighboring (I) in the QII fragment to an IQI sequence, a strictly alternating spatial arrangement of hydrophilic and lipophilic residues was obtained (Figure 3a, red model). In contrast to the PNF-1-6 series consisting of the KIKQII fragment, PNF-7 (CKIKIQINMWQ), PNF-8 (CKIKIQINM), and PNF-9 (CKIKIQI) now provide a facial amphiphilic character, where the positively charged and nonpolar residues are oriented not only in parallel but also perpendicular to the fibril axis. PNF-7 to PNF-9 with positive  $\zeta$ -potentials ( $\zeta = +10.7$ –22.3 mV) were formed with moderate to high CRs (54–87%) and showed the ability to enhance retroviral infection at 65  $\mu$ M, comparable to EF-C (Figure 3b–d; Figure S4, Supporting Information).

The corresponding (C)-free derivatives PNF-10 (KIKIQINMWQ) and PNF-11 (KIKIQINM) with the optimized KIKIQI patterns also assembled with high CRs (64–93%) into PNFs with positive  $\zeta$ -potentials ( $\zeta = +17.2$ –41.9 mV) that were however less active than EF-C in promoting retroviral infection. Interestingly, PNF-9 with only seven amino acids assembled into bioactive and positively charged PNFs ( $\zeta = +17.4$  mV, CR = 54%), whereas neutral PNF-3 ( $\zeta = +0.6$  mV) was inactive and PNF-6 and PNF-12 lacking the N-terminal (C) did not form fibrils (Figures 2c and 3c). These results indicate that the optimized amphiphilic CKIKIQI pattern of PNF-9 with N-terminal (C) represents the shortest sequence for forming positively charged PNFs displaying transduction enhancement in the range of EF-C.

Next, the (I) residues in PNF-9 were replaced by the less bulky and less hydrophobic alanine (A) and the sterically more demanding aromatic phenylalanine (F) residues. PNF-13 (CKAKAQANMWQ), PNF-14 (CKAKAQANM), and PNF-15 (CKAKAQQA) assembled into negatively charged PNFs ( $\zeta = -3.7$  to -9.1 mV) with high (PNF-13, 92%) to moderate CRs (PNF-14, PNF-15, 38–44%) that did not enhance viral transduction (Figure 3b–d). It has been reported that the aggregates of peptides with similar sequences can significantly vary in their  $\zeta$ -potential, often preventing a direct correlation between the peptide sequence and  $\zeta$ -potential.<sup>[49–51]</sup> The analogous lack in enhancing transduction was found after removing the N-terminal (C) of all three alanine derivatives resulting in PNF-S1 (KAKAQANMWQ), PNF-S2 (KAKAQANM), and PNF-S3 (KAKAQQA) (Figure S5, Supporting Information). In contrast, the (F)-containing derivatives PNF-16 (CKFKFQFNWQ), PNF-17 (CKFKFQFN), and PNF-18 (CKFKFQF) formed positively charged PNFs ( $\zeta = +14.1$ –22.3 mV) with high CRs (88–96%) (Figure 3b–d) that all showed significant transduction enhancement. Removal of the N-terminal (C) afforded PNF-S4 (KFKFQFNWQ) and PNF-S5 (KFKFQFN) displaying high transduction enhancement, whereas PNF-S6 (KFKFQF) was inactive (Figure S5, Supporting Information).

### 2.3. An N-Terminal Cysteine Improves Fibril Formation and Enhances Transduction

The impact of the N-terminal accessible thiol-residues was furthermore investigated by substitution of (C) in PNF-9 by the sulfur-containing amino acid methionine (M) in PNF-S7 (MKIKIQI). Both PNF-9 and PNF-S7 formed positively charged

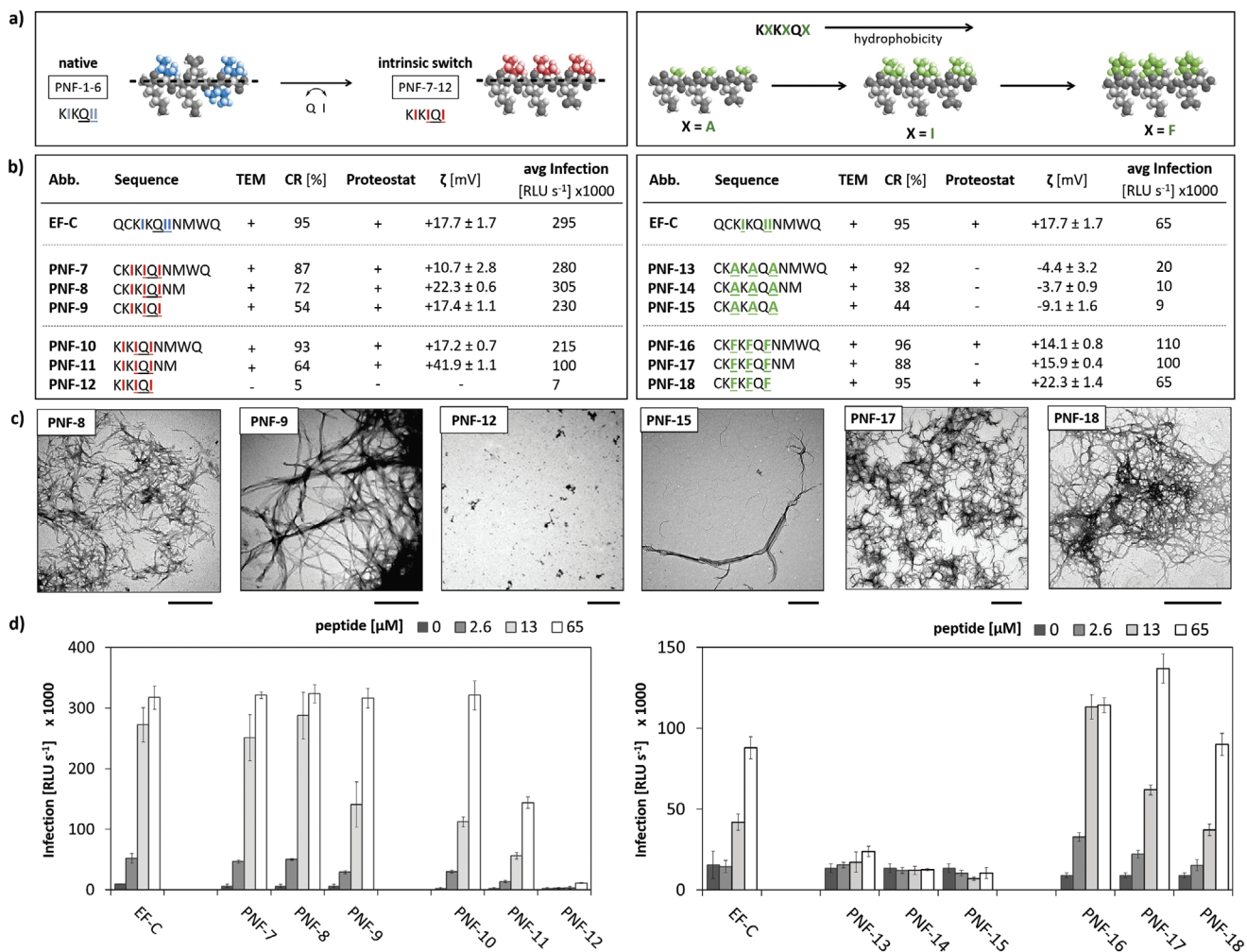


**Figure 3.** Improving PNF aggregating and transduction enhancement. a) Optimization of the amphiphilic fragment (II) of EF-C. Hydrophilic amino acids are given in grey and hydrophobic in color. b) Tabular summary of the features of PNF-7 to PNF-18 including PNF formation as observed in TEM measurements with + = fibrils and - = no aggregate formation detected. Monomer-to-fibril conversion rates (CR) were determined in a fluorescence-based assay. Proteostat emission indicates accessible cross  $\beta$ -sheet binding pockets in the fibril core and was assessed for PNFs with + = Proteostat activity and - = no Proteostat fluorescence observed.  $\zeta$ -potential values for PNF solutions. Average (avg) RLU s<sup>-1</sup> in infectivity assay for 13–65  $\mu$ M. c) Representative TEM micrographs of PNF-8, -9, -15, -17, -18 reveal fibrillar aggregate morphologies. No aggregates were observed for PNF-12. Scale bars: 500 nm. d) Transduction enhancement assay showing HIV-1 infection rates of TZM-bl cells observed in the presence of increasing concentrations of PNF given as mean values from triplicate infections  $\pm$  standard deviation. RLU s<sup>-1</sup>; relative light units per second.

nanofibrils of comparable morphology as confirmed by TEM measurements and both derivatives assembled with similar CRs (PNF-9, 54% and PNF-S7, 51%) (Figure S6, Supporting Information). However, PNF-S7 was significantly less bioactive than PNF-9 at all tested concentrations. The substitution of (C) by (M) in the shortest bioactive sequence PNF-18 afforded PNF-S8 (MKFKFQF), which was inactive (Figure S6, Supporting Information). The cysteine groups in the bioactive peptides could in principle undergo oxidation reactions under air, which could enhance the formation of disulfide bridges.<sup>[52]</sup> Therefore, we have studied bioactivity of PNF-8 in the presence of the reducing agent TCEP. Our data shows that the application of TCEP has no significant influence on bioactivity (Figure S7, Supporting Information). We conclude that in our study, N-terminal (C) leads to robust fibril formation and enhances infectivity also in case of short peptide sequences.

#### 2.4. Unraveling the Structure–Activity Relationship

We have shown that the formation of bioactive PNFs required moderate to high CR as well as an overall positive  $\zeta$ -potential. However, PNFs with similar positive charges and CRs, such as PNF-2 and PNF-5 could still reveal significantly different transduction enhancing activities (Figures 2 and 3). Therefore, CR and positive  $\zeta$ -potential represent critical features, but additional, yet unknown parameters exist that account for the observed variability in the biological activity of PNFs. To identify these parameters, we first correlated the sequence and transduction enhancement of PNFs with their secondary and quaternary structure that was obtained by FTIR spectroscopy (Figure 4) from freeze-dried PNF solutions. It has been shown that the properties of amyloid structures in a liquid and dried environment remain highly conserved.<sup>[53–55]</sup> In proteins, the IR spectra

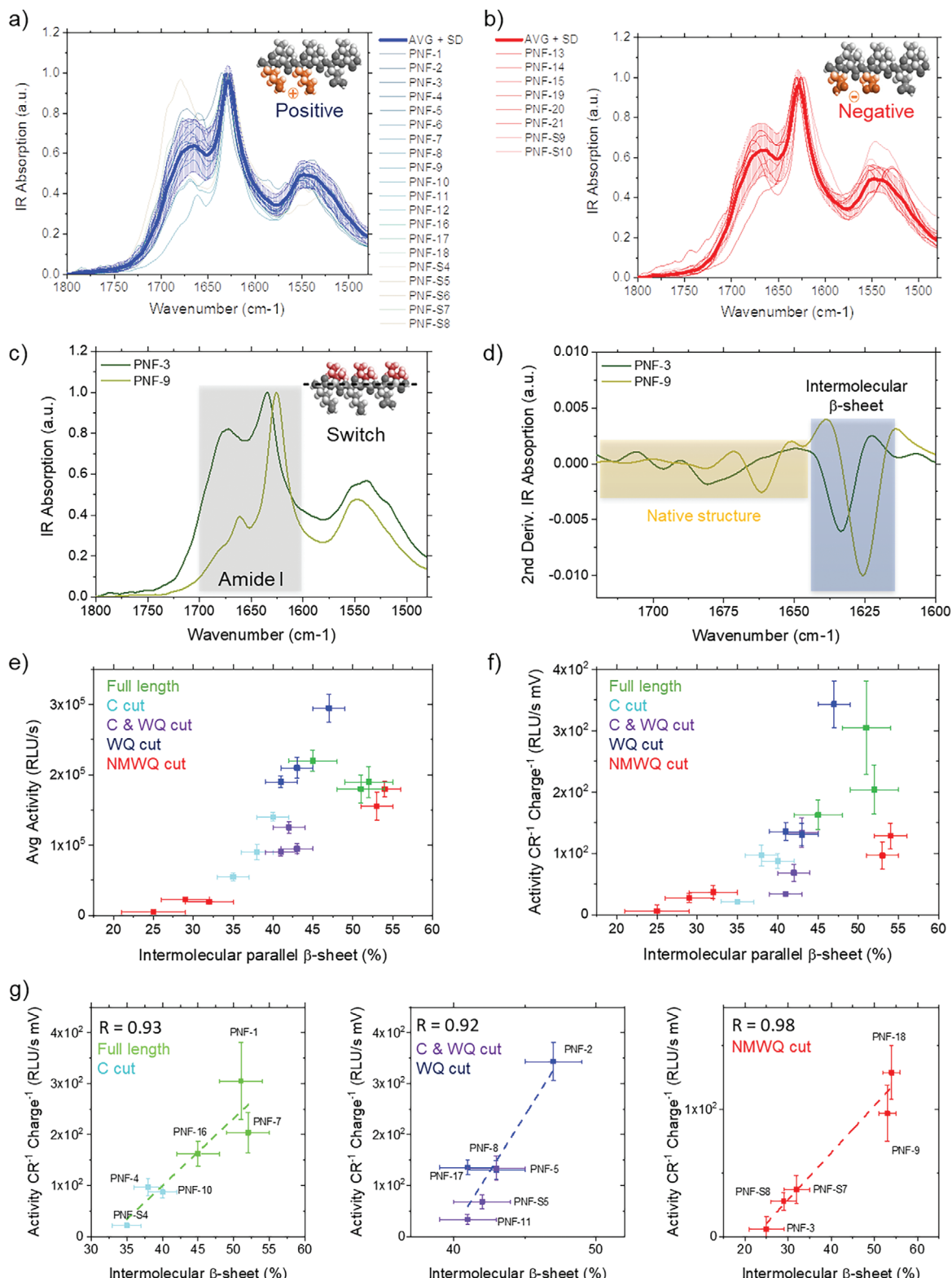


**Figure 4.** FTIR secondary structure evaluation and infectivity enhancement as a function of intermolecular  $\beta$ -sheet for all PNFs. FTIR spectra of a) positively and b) negatively charged PNFs. c) Modification of the amide band I upon intrinsic switch. d) Method of quantification of intramolecular versus intermolecular aggregated  $\beta$ -sheet structure. Secondary structure versus e) average infection enhancing activity and f) average infection enhancing activity normalized by charge and conversion rate. g) Linear fit of activity versus intermolecular  $\beta$ -sheet for the groups of peptides with chemical similarity. Full length: PNF-1,-7,-16; C cut: PNF-4,-10,-S4; C and WQ cut: PNF-5,-11,-S5; WQ cut: PNF-2,-8,-17; NMWQ cut: PNF-3,-9,-18,-S7,-S8.

are dominated by the amide band I, whose shape is intimately related to the secondary and quaternary structure of the protein backbone. A first qualitative view of the spectra shows that the amide band I of almost all PNFs exhibited a maximum in the range between  $1615\text{--}1630\text{ cm}^{-1}$  (Figure 4a,b). The high absorption in this spectroscopic range demonstrates the presence of a high content of intermolecular  $\beta$ -sheet structures, stabilized by a tight network of hydrogen bonds, similar to amyloidogenic aggregates.<sup>[56–58]</sup> Then, the integration of the deconvolved amide band I by a second derivative analysis allowed robust quantification of each structural contribution ( $\alpha$ -helix, random coil, native and aggregated  $\beta$ -sheet) (Figure 4c,d).<sup>[59,60]</sup> The percentage of native intramolecular secondary structural elements ( $1635\text{--}1700\text{ cm}^{-1}$ ) was quantified and correlated versus the percentage of intermolecular hydrogen bonded  $\beta$ -sheet ( $1610\text{--}1635\text{ cm}^{-1}$ ) for each PNF (Figure 4d).

The PNF library showed a wide variation of secondary structures as indicated by the heterogeneity of shapes of the amide band I of the PNFs (Figure 4a,b). The amide I band of the different negatively charged PNFs varied significantly (Figure 4b), and with similar standard deviation to the one of the positive PNFs (Figure 4a). However, there were no major differences in the secondary and quaternary structures of negatively charged PNFs that would explain the observed significant differences in their transduction enhancement compared to positively charged PNFs and the EF-C sequence. This observation is in line with previous reports indicating that the  $\zeta$ -potential of the PNFs is the first factor determining their transduction enhancing features.<sup>[17,18,61]</sup> However, positively charged PNFs revealed high variations in their structure and ability to boost transduction. An initial qualitative investigation of the spectra of these PNFs indicated that sequence modifications altered their secondary and quaternary structure, which also had an impact on their transduction enhancing features. For instance, the intrinsic switch of the core (Q) and (I) of PNF-3 (CKIKQII) leads to the formation of PNF-9 (CKIKIQI) with a higher content of intermolecular  $\beta$ -sheet structures that displayed improved transduction enhancing features (Figure 4c,d). The corresponding spectra showed that both in the presence and absence of the N-terminal cysteine (C), the intrinsic switch KIKQII  $\rightarrow$  KIKIQI allowed us to modulate with a higher degree of freedom the secondary structure of the PNFs upon the stepwise removal of WQ and NM amino acids (Figure S8, Supporting Information).

## 2.5. The Intermolecular $\beta$ -Sheet Content of PNFs Modulates their Transduction Efficiency

Next, we assessed how the molecular structure of the positively charged PNFs affects their impact on transduction efficiency. To reduce the intrinsic variability in the biological assay, the average transduction enhancement was calculated (Table S2, Supporting Information) and plotted as average biological activity against the content of the measured intermolecular  $\beta$ -sheet structures (Figure 4e). These data showed an unexpected and significant correlation as the biological activity increased steadily as a function of the intermolecular  $\beta$ -sheet content of the PNFs. As both charges and the CR are important

parameters contributing to transduction enhancement, we normalized our results against CR and  $\zeta$ -potential. Normalization for CR considers only the fraction of peptide monomers participating in PNF formation, whereas normalization for charge recognizes that only positively charged PNFs facilitate virus transport into cells (Figure 4f; Figure S9, Supporting Information). Interestingly, even after CR and charge normalization, a direct correlation between infectivity enhancement and the presence of intermolecular  $\beta$ -sheet content of the PNFs was observed.

To unravel the functional relationship between secondary structure and bioactivity, we also considered that the side chain absorption of the amino acids W, Q, and N can significantly contribute to the amide band I of a short peptide ( $\approx 5\text{--}15\%$ ). Thus, we grouped the peptides into three groups that are either chemically identical, that is, in case of structural isomers, or consist of amino acids, whose side chains do not affect the amide band I absorption. The plot of the  $\beta$ -sheet content versus infectivity for each of these groups revealed that these physical quantities are correlated by a statistically significant linear relationship (Figure 4g,  $R = 0.92\text{--}0.98$ ). These data clearly demonstrate that the content of the intermolecular  $\beta$ -sheet structures in the PNFs is a fundamental parameter modulating their infectivity (Figure 4g).

We observed above that (C) promotes enhanced transduction rates (Figure 2). The structural analysis revealed that deletion of C-terminal cysteine leads to a net average reduction of the intermolecular  $\beta$ -sheets content ( $\approx 15\%$ ) in the PNFs (Figure 4g, light blue PNF-4,-10,-S4 versus green PNF-1,-7,-16). Interestingly, the influence of the N-terminal (C) is not of a hydrophobic nature, as an exchange of (C) with the chemically similar (M) decreased the intermolecular  $\beta$ -sheets content and reduced infectivity in the corresponding peptides libraries (Figure 4g, red PNF-9, 18 to PNF-S7/-S8). Therefore, we found that the main role of the N-terminal (C) is to generate amyloid-like PNFs with a higher content of hydrogen bonded  $\beta$ -sheets and thus more stable PNFs with a higher degree of order,<sup>[45,62]</sup> which obviously enhances their infectivity.

Deletion of both the N-terminal (C) and the C-terminus had an impact on the content of intermolecular  $\beta$ -sheet, which also affected transduction. We observed that the N-terminal (C) or part of the C-terminus (NMWQ) is a necessary prerequisite for high infectivity of the EF-C sequence. Truncation of the C-terminal (WQ) sequence only slightly affected PNF infectivity (Figure 4f, green versus blue), and this minor difference in secondary structure was attributed to the absorption of the (WQ) side chains that were removed in the corresponding series PNF-2,-5,-8,-17,-S5. The removal of both (C) and C-terminal (WQ) sequence slightly reduced the intermolecular  $\beta$ -sheet content ( $\approx 5\%$ ), which also diminished infectivity enhancement (Figure 4g, blue PNF-4,-10,-S4 versus violet PNF-1,-7,-16), whereas deletion of (C) and the full C-terminus significantly reduced the intermolecular  $\beta$ -sheet content ( $\approx 20\%$ ), which resulted in an almost complete loss of the transduction enhancing features (Figure S10, Supporting Information).

As mentioned previously, the optimization of the amphiphilic pattern also resulted in significant changes in the secondary structure (Figure 4c,d). This effect was smaller for the sequences

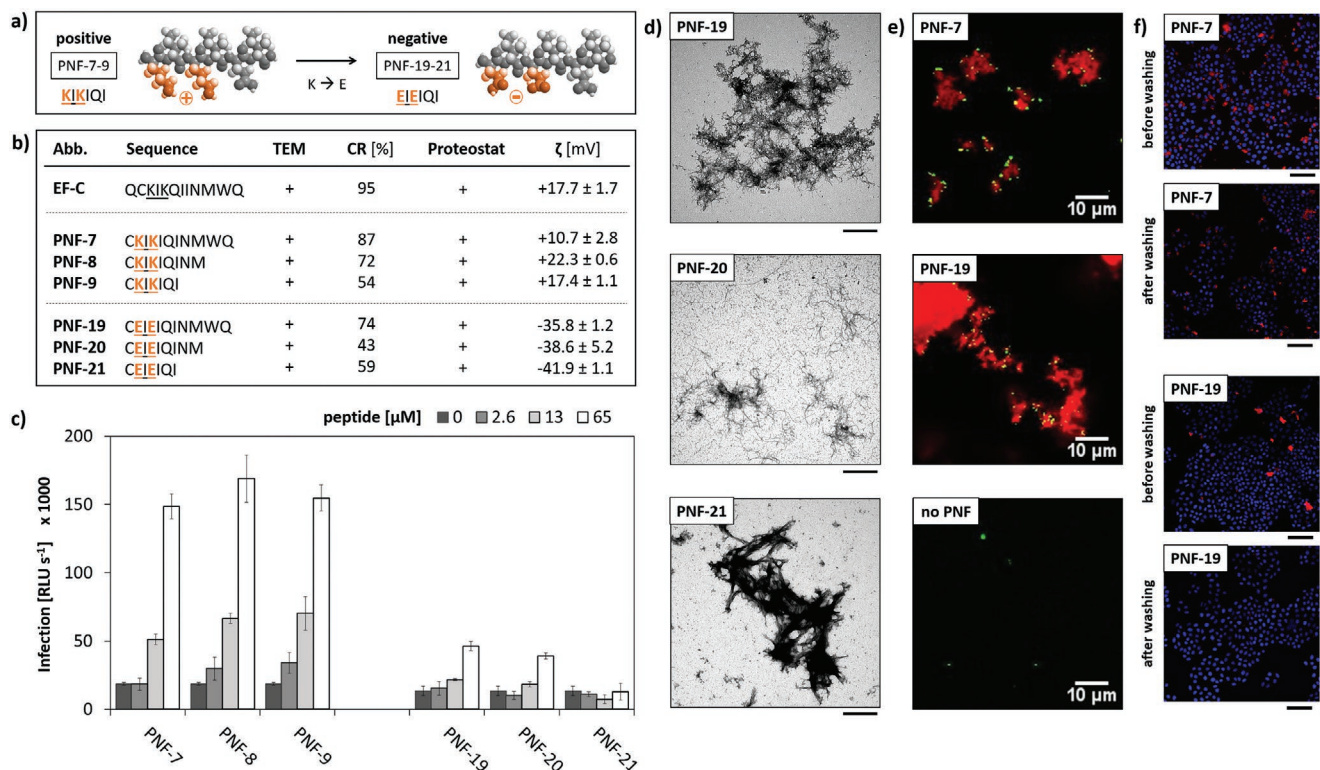


**Figure 5.** Variation of PNF charge from positive (bioactive) to negative (inactive). Both (K)-and (E)-rich fibrils bind virions, but the latter did not increase infectivity. a) Substitution of positively charged Lysine (K) residues by negatively charged glutamic acid (E) in the peptide sequences (PNF-7 to PNF-9) yielded corresponding negatively charged derivatives (PNF-19 to PNF-21) to elucidate the impact of PNF charge on self-assembly and infectivity enhancement. b) Tabular list of peptide derivatives PNF-19 to PNF-21 with glutamic acid residues and a positively charged lysine derivative set PNF-7 to PNF-9 including the ability to form PNFs as observed in TEM measurements with + = fibrils detected. Monomer-to-fibril conversion rates (CR) were determined in a fluorescence-based assay. High values indicate a large percentage of peptides participating in fibril formation. Proteostat emission indicates accessible cross  $\beta$ -sheet binding pockets in the fibril core and was assessed for PNFs with + = Proteostat activity and - = no Proteostat fluorescence observed.  $\zeta$ -potential values for PNF solutions confirm the negative charge of fibrillar aggregates with glutamic acid residues. c) Infectivity assay showing HIV-1 infection rates of TZM-bl cells observed in the presence of increasing concentrations of PNF. Values above the columns depict the change from baseline ( $0 \mu\text{M}$ ). Shown are mean values derived from triplicate infections  $\pm$  standard deviation. RLU  $\text{s}^{-1}$ ; relative light units per second. d) Representative TEM micrographs of PNF-19 to PNF-21 reveal fibrillar aggregate morphologies. The scale bars represent 500 nm. e) Representative LSM micrographs of Proteostat-labelled PNFs (red) incubated with YFP-labelled viral particles (green) revealed formation of mesoscale virus-PNF clusters for PNF-7 and PNF-19. f) Representative LSM micrographs of Proteostat-labelled PNFs (red) and TZM-bl cells (nucleus in blue). PNFs were added to cells for 30 min and analyzed. After 1 h, cells were washed and again analyzed. PNF-7 revealed association with cellular membranes while PNF-19 did not associate with cells. The scale bars represent 100  $\mu\text{m}$ .

close in length to EF-C and it became more pronounced for the highly truncated sequences, that is, those lacking the NMWQ fragment (Figure 4g, red). In these (C)-containing peptides, the intrinsic switch enabled the modulation of the secondary structure and their transduction enhancing features (Figure 4g, red). By optimizing the internal amphiphilic pattern of PNF-3, which afforded PNF-9, both  $\beta$ -sheet content and transduction efficiency received a significant boost (Figure 4g), which is in good agreement with an optimized packing of the molecules due to the elimination of a polarity “defect” in the structure. The effects delivered by the intrinsic switch were of similar importance, when considering the (F)-derivative peptides (PNF-18). This structure–activity relationship represents the first result clearly indicating that the molecular structure, and in particular the content of intermolecular  $\beta$ -sheet content, is a fundamental parameter determining the infectivity enhancing properties of peptide nanofibrils.

## 2.6. Negatively Charged PNFs Bind Virions but Not Cells

The positively charged (K) residues could be involved in interactions with negatively charged viral membranes and/or the negatively charged lipid bilayers of cellular membranes. In this way, positively charged PNFs could enhance virus transduction by reducing the electrostatic repulsion forces between viral and cellular membranes.<sup>[15,17]</sup> In order to elucidate the interaction partner of PNFs, negatively charged peptide sequences based on bioactive PNF-7 to PNF-9 were prepared in which the hydrophilic, polar (K) residue was replaced by glutamic acid (E). The corresponding derivatives PNF-19 (CEIEIQINMWQ), PNF-20 (CEIEIQINM), and PNF-21 (CEIEIQI) formed PNFs with negative zeta potentials with good CRs (43–79%), almost comparable to their corresponding positive (K)-derivatives PNF-7 to PNF-9. The CR of the negative (E)-peptides PNF-19 to PNF-21, but their biological activity was an order of magnitude smaller (Figure 5).

Next, we studied the formation of mesoscale virus-PNF clusters by applying fluorescent laser scanning microscopy (LSM). PNFs were stained by the red-emitting fluorophore Proteostat and yellow fluorescent protein (YFP)-labelled retroviral particles (green) were used. Colocalization of PNFs and virions was observed for all investigated PNFs as depicted in Figure 5e and Figure S11, Supporting Information, indicating that despite their negative charge, PNF-19 and PNF-21 were still able to bind virions, although to a lower extent as their positively charged analogues. The interaction of PNFs with cellular membranes was then assessed by incubating Proteostat-labelled PNFs with TZM-bl cells for 30 min. The samples were analyzed by confocal microscopy before washing confirming the presence of PNF. After 1 h, cells were washed with PBS and examined again. PNF clusters were removed that did not significantly interact with the cellular surface. In contrast to (K)-containing PNFs, negatively charged PNFs based on optimized peptide sequences interacted with virions but they did not associate with the cellular membrane (Figure S12, Supporting Information), which most likely explains their lack of activity in the transduction assay (Figure 5c). The (K) residues in the bioactive PNFs reveal enhanced virus binding and facilitate colocalization of the virus-PNF complexes at cellular membranes. Interestingly, a set of peptides PNF-S9 and PNF-S10, where the charged residues were replaced with serine (S) (Figure S13, Supporting Information), show intermediate activity roughly between that of the highly active (K)-containing PNFs and the non-active (E)-containing PNFs. Colocalization of these PNFs and viral particles indicated poor attachment to cellular membranes confirming the overall importance of positively charged residues to enhance viral transduction efficacy. We conclude that a positive  $\zeta$ -potential is crucial for the transduction enhancing properties of PNFs but it is not essential for PNF assembly and interaction with virions.

## 2.7. The Shortest Transduction Enhancing Sequence PNF-18 is a Potent Enhancer of Lenti- and $\gamma$ -Retroviral Transduction

The peptide PNF-18 is a highly efficient transduction enhancer providing a short sequence of only seven amino acids. We selected this hit peptide for a comparative analysis with the EF-C 12-mer using multiple viral vectors and cell lines (Figure 6a). A lentiviral vector encoding a luciferase gene and carrying the G-protein of the vesicular stomatitis virus (VSV-G), a viral fusion protein often used in gene transfer approaches, was generated. p24 antigen of the viral pseudotype preparation (2 or 14 ng) were exposed to EF-C and PNF-18, and used to inoculate HEK 293T cells. Transduction efficiencies were determined 3 days later by quantifying luciferase activities in cellular lysates. Both PNFs substantially increased transduction (Figure 6b). At 100  $\mu$ g mL<sup>-1</sup>, PNF-18 is more active than EF-C, with maximal transduction enhancement of 32-fold (2 ng p24) and 17 $\times$  (14 ng p24), as compared to 23 $\times$  (2 ng p24) and 10 $\times$  (14 ng p24), respectively, for EF-C. We also generated a lentiviral vector, SEW LUC2, by co-transfection of a crippled lentiviral genome encoding luciferase, a gag-pol and a VSV-G expression plasmid. The resulting vector was treated with EF-C and PNF-18, and mixtures were added to HeLa (TZM-bl) cells

and murine fibroblast 3T3 cells. Again, transduction rates were determined by quantifying luciferase 3 days later. As shown in Figure 6c, both PNF dose-dependently increased transduction of both cell lines analyzed. PNF-18 revealed maximal enhancement of 121-fold in TZM-bl cells and 66-fold in 3T3 cells. Since one of the most advanced clinical applications of PNF is to increase retroviral transduction of T cells in CAR T cell therapy,<sup>[34,63]</sup> we finally evaluated PNF-18 in this setting. For this, a GFP encoding retroviral vector carrying the Env protein of the Gibbon ape leukemia virus (GALV-Env) which is commonly used in CAR T cell therapy was generated, without applying any optimization protocols or virion concentration by ultracentrifugation. Next, the vector was exposed to PNF-18 and added to primary T cells isolated from two independent blood donors. Transduction rates were analyzed 3 days later by determining the percentage of GFP+ cells by flow cytometry (Figure 6d,e). In the absence of PNFs, hardly any transduced GFP+ cells were detected. However, with an increasing concentration of PNF-18, the number of transduced cells gradually increased to 9.5% for donor A, and 7.2% for donor B (Figure 6d), corresponding to 63 or 48-fold increased transduction rates as compared to the control containing no PNFs (Figure 6e). These results show, that fibrils derived from the 7-mer peptide PNF-18 substantially improved lentiviral gene transfer rates into adherent and primary suspension cells, independently of the viral fusion protein and the vector types used, rendering PNF-18 as a novel highly versatile and easy to produce transduction enhancer.

## 3. Conclusions

Supramolecular nanostructures are notoriously challenging to optimize as rational approaches face multiparameter and multiscale challenges. Herein, we have reported the first sequence optimization of peptides forming bioactive amyloid-like PNFs that enhance retroviral gene transduction based on single fibril analysis and quantitative infection data. The impact of different amino acid patterns and sequences responsible for assembly, fibril morphologies, virus and cell membrane binding were resolved. We found that the motif NMWQ in QCKIKQIINMWQ was not essential for their transduction enhancing properties. Optimizing the amphiphilic six amino acid sequence (KIKQII) afforded (CKFKFQF) with quantitative peptide-to-fibril CRs. The N-terminal (C) also affected fibril morphology by further increasing the intermolecular  $\beta$ -sheet content, which also contributed to high transduction efficacy in particular in short sequences. The structure–activity relationship showed a linear correlation of the content of intermolecular  $\beta$ -sheet structures and transduction enhancement of the PNFs. The (K)-residues were found important for binding both virions and cell surface structures by reducing the electrostatic repulsion forces between viral and cellular membranes to colocalize virions at the cellular membrane, which is required for transduction enhancement. Interestingly, negatively charged PNFs with optimized sequence patterns could still bind virions but the formed negative PNF-virion complexes did not co-localize with cellular membranes.

The nine-mers PNF-8 and PNF-17 as well as the seven-mer PNF-18 (CKFKFQF) represent a minimum sequence

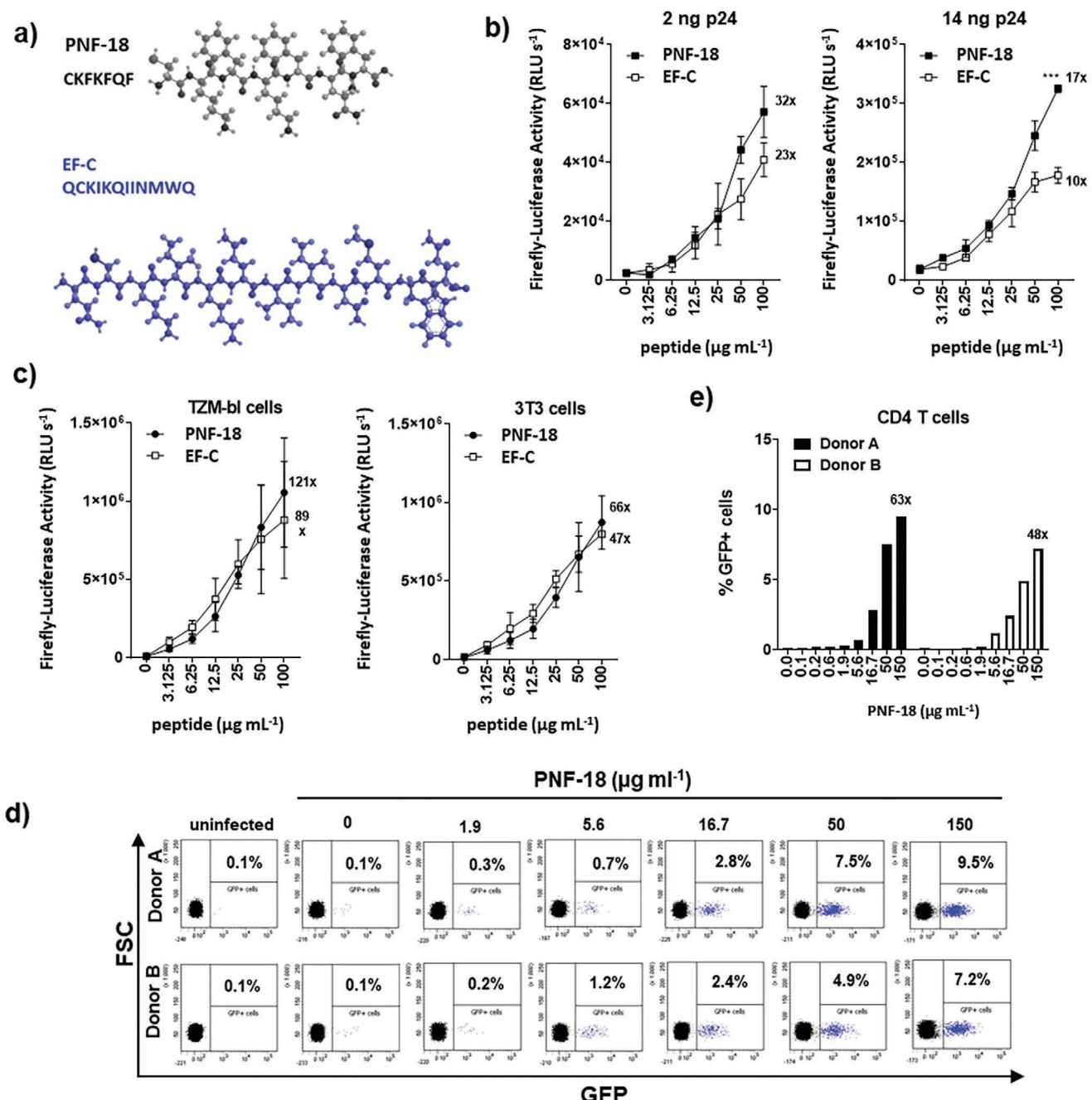


**Figure 6.** Fibrils derived from the shortened peptide PNF-18 are potent enhancer of lenti- and  $\gamma$ retroviral transduction. a) Structure of PNF-18 and the parental EF-C peptide. b) Transduction efficiencies of a low (left) or median (right) dose of VSV-G pseudotyped HIV-1 NL4-3 particles encoding a luciferase. Viral particles were exposed to the indicated concentrations of EF-C and PNF-18 and used to inoculate HEK 293T cells. Luciferase activities were determined three days later, shown are mean values derived from triplicate infection  $\pm$  standard deviation (SD). c) Transduction efficiencies of a VSV-G pseudotyped lentiviral vector (SEW LUC2) in TZM-bl or 3T3 cells. The SEW LUC2 vector preparation was incubated with the PNF and used to infect TZM-bl and 3T3 cells. Luciferases activities were determined 3 days later, shown are mean values derived from triplicate infections  $\pm$  SD. d) Dot plots showing GFP+ CD4 T cells obtained from two independent donors after transduction with GALV pseudotyped  $\gamma$ retrovirus at indicated concentrations of PNF-18 at three days post transduction. e) Percentage of GFP positive cells shown in (d). Numbers above data points give the *n*-fold enhancement of transduction as compared to controls containing no PNF.

combining PNF formation with high CRs and high infectivity due to: 1) high content of cross- $\beta$ -sheet structures; 2) ability to bind virions; and 3) interact with cellular membranes. PNF-18 provides a more than 40% reduced sequence length compared

to the original 12-mer EF-C sequence promoting optimized lentiviral HIV infection and enhanced retroviral transduction with high efficiency outperforming the original EF-C sequence. PNF-18 is less expensive to synthesize, it can be purified and

produced without batch-to-batch variations and it further provides reactive thiol groups to introduce further chemical modifications, that is, via maleimide chemistry. We envision that negatively charged (E)-based PNFs capable of binding viral particles without interacting with cellular membranes could offer exciting opportunities to develop antiviral nanomaterials as well as PNFs targeting specific cell types as positive charges usually mediate unspecific electrostatic interactions with cellular membranes.

## Supporting Information

Supporting Information is available from the Wiley Online Library or from the author.

## Acknowledgements

S.S. and T.M. contributed equally to this work. The project was funded by the German Research Foundation (DFG) – project number 316249678 – CRC 1279 (A03, A05, C01). T.W., J.M., and F.K. acknowledge funding by the Volkswagen Foundation (project 89943) and J.M. by the Leibniz Association (SAW project). The authors thank Jasmina Gačanin for assisting in peptide synthesis and Nicole Kirsch-Pietz in proofreading.

Open access funding enabled and organized by Projekt DEAL.

## Conflict of Interest

The authors declare no conflict of interest.

## Data Availability Statement

Data available on request from the authors.

## Keywords

peptide nanofibrils, retroviral gene transfer, self-assembly, structure-activity relationship

Received: November 3, 2020

Revised: January 20, 2021

Published online: February 22, 2021

- [1] T. P. J. Knowles, J. F. Smith, G. L. Devlin, C. M. Dobson, M. E. Welland, *Nanotechnology* **2007**, *18*, 044031.
- [2] T. Lührs, C. Ritter, M. Adrian, D. Riek-Loher, B. Bohrmann, H. Do, D. Schubert, R. Riek, *Proc. Natl. Acad. Sci. USA* **2005**, *102*, 17342.
- [3] L. C. Serpell, *Biochim. Biophys. Acta, Mol. Basis Dis.* **2000**, *1502*, 16.
- [4] G. Wei, Z. Su, N. P. Reynolds, P. Arosio, I. W. Hamley, E. Gazit, R. Mezzenga, *Chem. Soc. Rev.* **2017**, *46*, 4661.
- [5] I. Cherny, E. Gazit, *Angew. Chem., Int. Ed.* **2008**, *47*, 4062.
- [6] Z. Xu, R. Paparcone, M. J. Buehler, *Biophys. J.* **2010**, *98*, 2053.
- [7] D. M. Fowler, A. V. Koulov, C. Alory-Jost, M. S. Marks, W. E. Balch, J. W. Kelly, *PLoS Biol.* **2006**, *4*, 0100.
- [8] S. K. Maji, D. Schubert, C. Rivier, S. Lee, J. E. Rivier, R. Riek, *PLoS Biol.* **2008**, *6*, e17.
- [9] N. R. Roan, N. Sandi-Monroy, N. Kohgadai, S. M. Usmani, K. G. Hamil, J. Neidleman, M. Montano, L. Ständker, A. Röcker,

- M. Cavrois, J. Rosen, K. Marson, J. F. Smith, C. D. Pilcher, F. Gagsteiger, O. Sakk, M. O'Rand, P. V. Lishko, F. Kirchhoff, J. Münch, W. C. Greene, *Elife* **2017**, *6*, e24888.
- [10] M. R. Chapman, L. S. Robinson, J. S. Pinkner, R. Roth, J. Heuser, M. Hammar, S. Normark, S. J. Hultgren, *Science* **2002**, *295*, 851.
- [11] T. P. J. Knowles, M. Vendruscolo, C. M. Dobson, *Nat. Rev. Mol. Cell Biol.* **2014**, *15*, 384.
- [12] N. R. Roan, H. Liu, S. M. Usmani, J. Neidleman, J. A. Muller, A. Avila-Herrera, A. Gawanbacht, O. Zirafi, S. Chu, M. Dong, S. T. Kumar, J. F. Smith, K. S. Pollard, M. Fandrich, F. Kirchhoff, J. Munch, H. E. Witkowska, W. C. Greene, *J. Virol.* **2014**, *88*, 7221.
- [13] S. M. Usmani, O. Zirafi, J. A. Müller, N. L. Sandi-Monroy, J. K. Yadav, C. Meier, T. Weil, N. R. Roan, W. C. Greene, P. Walther, K. P. R. Nilsson, P. Hammarström, R. Wetzel, C. D. Pilcher, F. Gagsteiger, M. Fandrich, F. Kirchhoff, J. Münch, *Nat. Commun.* **2014**, *5*, 3508.
- [14] J. Münch, E. Rücker, L. Ständker, K. Adermann, C. Goffinet, M. Schindler, S. Wildum, R. Chinnadurai, D. Rajan, A. Specht, G. Giménez-Gallego, P. C. Sánchez, D. M. Fowler, A. Koulov, J. W. Kelly, W. Mothes, J. C. Grivel, L. Margolis, O. T. Keppler, W. G. Forssmann, F. Kirchhoff, *Cell* **2007**, *131*, 1059.
- [15] A. Röcker, N. R. Roan, J. K. Yadav, M. Fandrich, J. Münch, *Chem. Commun.* **2018**, *54*, 7557.
- [16] K. Kaygisiz, C. V. Synatschke, *Biomater. Sci.* **2020**, *8*, 6113.
- [17] C. Meier, T. Weil, F. Kirchhoff, J. Münch, *Wiley Interdiscip. Rev.: Nanomed. Nanobiotechnol.* **2014**, *6*, 438.
- [18] M. Yolamanova, C. Meier, A. K. Shaytan, V. Vas, C. W. Bertoncini, F. Arnold, O. Zirafi, S. M. Usmani, J. A. Müller, D. Sauter, C. Goffinet, D. Palesch, P. Walther, N. R. Roan, H. Geiger, O. Lunov, T. Simmet, J. Bohne, H. Schrezenmeier, K. Schwarz, L. Ständker, W.-G. Forssmann, X. Salvatella, P. G. Khalatur, A. R. Khokhlov, T. P. J. Knowles, T. Weil, F. Kirchhoff, J. Münch, *Nat. Nanotechnol.* **2013**, *8*, 130.
- [19] E. Montini, D. Cesana, M. Schmidt, F. Sanvito, M. Ponzoni, C. Bartholomae, L. S. Sergi, F. Benedicenti, A. Ambrosi, C. Di Serio, C. Doglioni, C. Von Kalle, L. Naldini, *Nat. Biotechnol.* **2006**, *24*, 687.
- [20] L. Naldini, U. Blömer, P. Gallay, D. Ory, R. Mulligan, F. H. Gage, I. M. Verma, D. Trono, *Science* **1996**, *272*, 263.
- [21] S. L. Ginn, A. K. Amaya, I. E. Alexander, M. Edelstein, M. R. Abedi, *J. Gene Med.* **2018**, *20*, e3015.
- [22] P. Kumar, C. Woon-Khiong, *Curr. Gene Ther.* **2011**, *11*, 144.
- [23] T. Sakuma, M. A. Barry, Y. Ikeda, *Biochem. J.* **2012**, *443*, 603.
- [24] A. Biffi, E. Montini, L. Lorioli, M. Cesani, F. Fumagalli, T. Plati, C. Baldoli, S. Martino, A. Calabria, S. Canale, F. Benedicenti, G. Vallanti, L. Biasco, S. Leo, N. Kabbara, G. Zanetti, W. B. Rizzo, N. A. L. Mehta, M. P. Cicalese, M. Casiraghi, J. J. Boelens, U. Del Carro, D. J. Dow, M. Schmidt, A. Assanelli, V. Neduvia, C. Di Serio, E. Stupka, J. Gardner, C. Von Kalle, C. Bordignon, F. Ciceri, A. Rovelli, M. G. Roncarolo, A. Auti, M. Sessa, L. Naldini, *Science* **2013**, *341*, 1233158.
- [25] L. W. Seymour, A. J. Thrasher, *Nat. Biotechnol.* **2012**, *30*, 588.
- [26] H. Hanenberg, K. Hashino, H. Konishi, A. R. Hock, I. Kato, D. A. Williams, *Hum. Gene Ther.* **1997**, *2206*, 2193.
- [27] T. Moritz, P. Dutt, X. Xiao, D. Carstanjen, T. Vik, H. Hanenberg, D. A. Williams, *Blood* **1996**, *88*, 855.
- [28] A. Quintás-Cardama, R. K. Yeh, D. Hollyman, J. Stefanski, C. Taylor, Y. Nikhamin, G. Imperato, M. Sadelain, I. Rivièrè, R. J. Brentjens, *Hum. Gene Ther.* **2007**, *18*, 1253.
- [29] P. Zhou, J. Lee, P. Moore, K. M. Brasky, *Hum. Gene Ther.* **2001**, *12*, 1843.
- [30] K. Dodo, H. Chono, N. Saito, Y. Tanaka, K. Tahara, I. Nukaya, J. Mineno, *PLoS One* **2014**, *9*, e86275.
- [31] C. H. J. Lamers, P. van Elzakker, S. C. L. van Steenbergen, S. Sleijfer, R. Debets, J. W. Gratama, *Cytotherapy* **2008**, *10*, 406.
- [32] T. Tsukamoto, S. Okada, *J. Virol. Methods* **2017**, *248*, 234.

- [33] H. J. Lee, Y. S. Lee, H. S. Kim, Y. K. Kim, J. H. Kim, S. H. Jeon, H. W. Lee, S. Kim, H. Miyoshi, H. M. Chung, D. K. Kim, *Biologicals* **2009**, *37*, 203.
- [34] A. Castro, M. Drosch, M. Liesenfeld, T. Kaan, A. Schilz, H. Wenschuh, W. Forsmann, K. Kuhlke, *Cytotherapy* **2019**, *21*, e14.
- [35] D. Fenard, D. Ingrao, A. Seye, J. Buisset, S. Genries, S. Martin, A. Kichler, A. Galy, *Mol. Ther.–Nucleic Acids* **2013**, *2*, e90.
- [36] D. Schuetz, S. Rode, C. Read, J. Mueller, B. Glocker, K. Sparrer, O. Fackler, P. Walther, J. Muench, bioRxiv <https://doi.org/10.1101/2020.10.01.321810>.
- [37] J. Chen, R. Ren, S. Tan, W. Zhang, X. Zhang, F. Yu, T. Xun, S. Jiang, S. Liu, L. Li, *PLoS One* **2015**, *10*, e0144522.
- [38] J. Chen, R. Ren, F. Yu, C. Wang, X. Zhang, W. Li, S. Tan, S. Jiang, S. Liu, L. Li, *Biophys. J.* **2017**, *113*, 1425.
- [39] S. Tan, L. Li, L. Lu, C. Pan, H. Lu, Y. Oksov, X. Tang, S. Jiang, S. Liu, *FEBS Lett.* **2014**, *588*, 1515.
- [40] H. Zhang, X. He, Y. Shi, Y. Yu, S. Guan, X. Gong, H. Yin, Z. Kuai, Y. Shan, *RSC Adv.* **2016**, *6*, 82082.
- [41] R. Franke, T. Hirsch, J. Eichler, *J. Recept. Signal Transduction* **2006**, *26*, 453.
- [42] C. Schilling, T. Mack, S. Lickfett, S. Sieste, F. S. Ruggeri, T. Sneideris, A. Dutta, T. Bereau, R. Naraghi, D. Sinske, T. P. J. Knowles, C. V. Synatschke, T. Weil, B. Knöll, *Adv. Funct. Mater.* **2019**, *29*, 1809112.
- [43] S. Navarro, S. Ventura, *Biotechnol. J.* **2014**, *9*, 1259.
- [44] E. J. Platt, K. Wehrly, S. E. Kuhmann, B. Chesebro, D. Kabat, *J. Virol.* **1998**, *72*, 2855.
- [45] J. Adamcik, F. S. Ruggeri, J. T. Berryman, A. Zhang, T. P. J. Knowles, R. Mezzenga, *Adv. Sci.* **2020**, *8*, 2002182.
- [46] V. Castelletto, P. Ryumin, R. Cramer, I. W. Hamley, M. Taylor, D. Allsop, M. Reza, J. Ruokolainen, T. Arnold, D. Hermida-Merino, C. I. Garcia, M. C. Leal, E. Castaño, *Sci. Rep.* **2017**, *7*, 43637.
- [47] R. J. Betush, J. M. Urban, B. L. Nilsson, *Pept. Sci.* **2018**, *110*, e23099.
- [48] F. T. Senguen, N. R. Lee, X. Gu, D. M. Ryan, T. M. Doran, E. A. Anderson, B. L. Nilsson, *Mol. BioSyst.* **2011**, *7*, 486.
- [49] Y. Chen, H. X. Gan, Y. W. Tong, *Macromolecules* **2015**, *48*, 2647.
- [50] S. Toksoz, R. Mammadov, A. B. Tekinay, M. O. Guler, *J. Colloid Interface Sci.* **2011**, *356*, 131.
- [51] T. A. Martinek, A. Hetényi, L. Fülöp, I. M. Mándity, G. K. Tóth, I. Dékány, F. Fülöp, *Angew. Chem.* **2006**, *118*, 2456.
- [52] R. Honda, *Biophys. J.* **2018**, *114*, 885.
- [53] F. S. Ruggeri, P. Flagmeier, J. R. Kumita, G. Meisl, D. Y. Chirgadze, M. N. Bongiovanni, T. P. J. Knowles, C. M. Dobson, *ACS Nano* **2020**, *14*, 5213.
- [54] K. Baginska, J. Makowska, W. Wiczka, F. Kasprzykowski, L. Chmurzynski, *J. Pept. Sci.* **2008**, *14*, 283.
- [55] A. Adochitei, G. Drochioiu, *Rev. Roum. Chim.* **2011**, *56*, 783.
- [56] V. Cabiaux, R. Brasseur, R. Wattiez, P. Falmagne, J. M. Ruysschaert, E. Goormaghtigh, *J. Biol. Chem.* **1989**, *264*, 4928.
- [57] E. Goormaghtigh, V. Cabiaux, J. Ruysschaert, *Eur. J. Biochem.* **1990**, *193*, 409.
- [58] D. M. Byler, H. Susi, *Biopolymers* **1986**, *25*, 469.
- [59] F. S. Ruggeri, B. Mannini, R. Schmid, M. Vendruscolo, T. P. J. Knowles, *Nat. Commun.* **2020**, *11*, 2945.
- [60] F. S. Ruggeri, G. Longo, S. Faggiano, E. Lipiec, A. Pastore, G. Dietler, *Nat. Commun.* **2015**, *6*, 7831.
- [61] N. R. Roan, J. Münch, N. Arhel, W. Mothes, J. Neidleman, A. Kobayashi, K. Smith-McCune, F. Kirchhoff, W. C. Greene, *J. Virol.* **2009**, *83*, 73.
- [62] F. S. Ruggeri, J. Adamcik, J. S. Jeong, H. A. Lashuel, R. Mezzenga, G. Dietler, *Angew. Chem., Int. Ed.* **2015**, *54*, 2462.
- [63] A. Jamali, L. Kapitza, T. Schaser, I. C. D. Johnston, C. J. Buchholz, J. Hartmann, *Mol. Ther.–Methods Clin. Dev.* **2019**, *13*, 371.